Volume 1 | Number 1 | Jan 2013 | Pages 1–100

PCCP

Physical Chemistry Chemical Physics
www.rsc.org/pccp

ROYAL SOCIETY OF CHEMISTRY

ROYAL SOCIETY OF CHEMISTRY

www.rsc.org/pccp

Journal Name

RSCPublishing

ARTICLE

Facile preparation of a photoactivatable surface on a 96-well plate: a versatile and multiplex cell migration assay platform

Masao Kamimura,[a] Olivia Scheideler,[a,b] Yoshihisa Shimizu,[a] Shota Yamamoto,[c] Kazuo Yamaguchi,[c] and Jun Nakanishi *[a]

Cell migration is an essential cellular activity in various physiological and pathological processes, such as wound healing and cancer metastasis. Therefore, *in vitro* cell migration assays are important not only for fundamental biological studies but also for evaluating potential drugs that control cell migration activity in medical applications. In this regard, robust control over cell migrating microenvironments is critical for reliable and quantitative analysis as cell migration is highly dependent upon the microenvironments. Here, we developed a facile method for making a commercial glass-bottom 96-well plate photoactivatable for cell adhesion, aiming to develop a versatile and multiplex cell migration assay platform. Cationic poly-D-lysine was adsorbed to the anionic glass surface via electrostatic interactions and, subsequently, functionalized with poly(ethylene glycol) (PEG) bearing a photocleavable reactive group. The initial PEGylated surface is non-cell-adhesive. However, upon near-ultraviolet (UV) irradiation, the photorelease of PEG switches the surface from non-biofouling to cell-adhesive. With this platform, we assayed cell migration in the following procedure: (1) create cell-attaching regions of precise geometries by controlled photoirradiation, (2) seed cells to allow them to attach selectively to the irradiated regions, (3) UV expose the remaining PEGylated regions to extend the cell-adhesive area, (4) analyse cell migration with microscopy. Surface modification of the glass surface was characterized by ζ-potential and contact angle measurements. The PEGylated surface showed cell-resistivity and became cell-adhesive upon releasing PEG by near-UV irradiation. The method was applied for parallelly evaluating the effect of model drugs on migration of epithelial MDCK cells in the multiplexed platform. Dose-response relationship for the cytochalasin D treatment on cell migration behavior was successfully evaluated with high reproducibility. Interestingly, the impact of blebbistatin on cell migration was dependent upon the widths of the migrating regions, resulting in both cases of migration acceleration and deceleration. These results clearly demonstrate that the cellular response to certain drugs is highly affected by their migrating geometries. Therefore, the obtained novel photoactivatable 96-well plate serves as a useful high-throughput platform for the identification of drug candidates that have an effect on cell migration behavior.

Introduction

Cellular migration is a dynamic process that underlies a variety of key physiological events, such as morphogenesis, immune response, and wound healing, and has also been demonstrated to play a central role in cancer invasion and metastasis.[1-4] To date, numerous *in vitro* migration assays have been developed to dissect the molecular mechanisms of cell migration as well as to serve as tools for discovering new drugs that regulate cell migration and block tumor expansion.[5,6] Recently, however, the desire for high-throughput screening (HTS) systems for

identifying new drug candidates have stimulated a demand for new platforms of multiplex assay formats. These screening techniques greatly contribute to the development of new pharmaceuticals by allowing for the evaluation of drug potencies and efficacies in terms of their ability to change cell migration rates.[7-12] Additionally, multiplex assay platforms have proven to be useful for functional genomics, (i.e. siRNA screening) to identify proteins involved in cell migration.[13] The ability to evaluate migration phenotypes, such as cell morphology as well as directional persistence and collectivity, represents another important objective when elucidating cell

Physical Chemistry Chemical Physics Accepted Manuscript
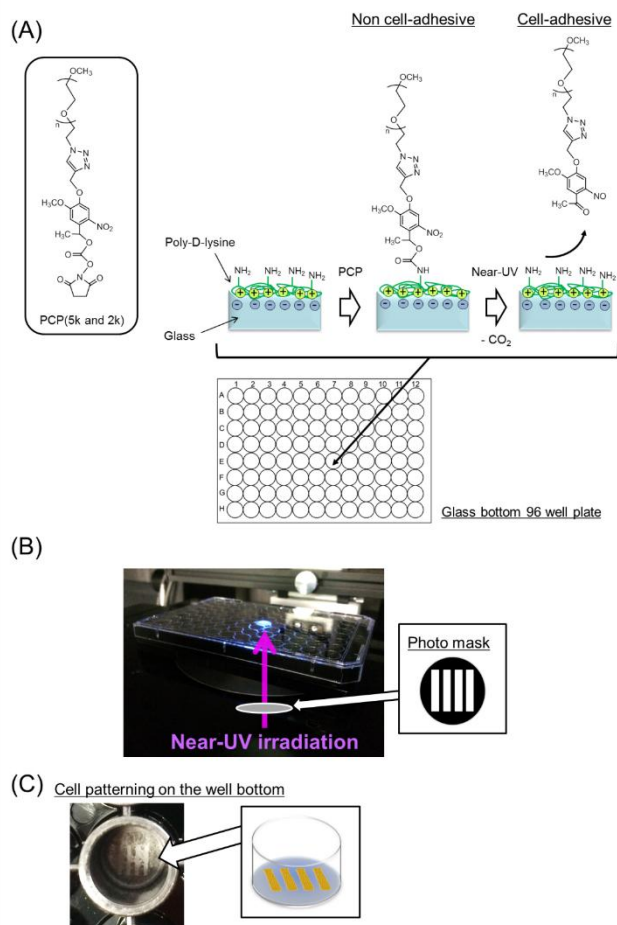
Fig. 1 Schematic illustrations of photoactivatable surface on the 96-well glass bottom plate. (A) Surface functionalization and the photoactivation procedure. (B) A picture of the photoirradiation step. (C) Striped cell patterns formed on the 96-well glass bottom plate can be seen even by naked eyes after dryness.

migration machinery. Recent studies have demonstrated that cellular microenvironments, or geometrical constraints, are critical in determining the mode of collective migration or leader cell formation.[14,15] In consideration of the broad range of *in vivo* external constraints and the dynamic features of cellular microenvironments,[16] it is important to engineer novel multiplex cell migration assay platforms where cellular geometrical constraints can be taken into consideration.

Conventional wound healing assays[17-20] and relatively-recent exclusion zone assays[21-24] have been used to evaluate migration kinetics as well as phenotypes based on the shared strategy of inducing cell migration. Other cell migration assays based on microfluidics devices[25,26] and magnetic levitation methods[7] have also been reported. However, the impact of geometrical constraints on cell migration ability as well as phenotypes is less significant in these methods, especially in HTS platforms. Thus, cell migration is usually evaluated in simple migration modes, such as cluster expansion or wound closure. In this regard, dynamic substrates serve as ideal platforms for cell migration assays, which allow for precise control over the cells' migrating microenvironments.[3,27-30] Cellular adhesion to these dynamic substrates can be controlled via the application of an

external stimulus, such as temperature,[31,32] voltage,[33-35] or light.[36-41] These dynamic substrates allow for inducing cell migration from and/or along controlled geometrical confinements with a well-defined migration frontier. Among them, light-responsive dynamic substrates possess several distinct advantages for cellular patterning in terms of their high spatial and temporal resolutions. These features allow for the preparation of cell migration assay platform in well-defined microenvironment depending on users' purposes.

Our group has reported the development of photoactivatable dynamic substrates based on silane-coupling agents bearing a photocleavable 2-nitrobenzyl ester.[15,42-51] Glass substrates functionalized with the photocleavable reagents and blocking agents, such as bovine serum albumin (BSA),[44-46] pluronic,[47] and poly(ethylene glycol) (PEG), change from non-cell-adhesive to cell-adhesive in response to near-ultraviolet (UV) irradiation.[15,48-52] Various geometrically-controlled single cells as well as cell clusters can be created by simple photoirradiation under a standard fluorescence microscope, and their migration to the previously idle areas can be induced by extending cell-adhesive areas by a secondary irradiation. Thus, photoactivatable dynamic substrates offer a versatile platform for cell migration assays with consideration of cellular microenvironments. It would be straightforward to bond a photoactivatable glass coverslip with a plastic plate with multiple bottomless wells (like, 96-well or 384-well) to develop a multiplex cell migration assay platform. However, photocurable resins are usually used to prepare multi-well plates in the commercialization processes, and our photoactivatable substrates are susceptible to the near-UV light used in this curing step. In addition, *in situ* silanization of commercial glass-bottom plates is not suitable since our photocleavable silanes dissolve only in organic solvents, which erode the plastic as well as the adhesion bond between the plastic and the glass substrate. To address these pitfalls, we herein developed an alternative, simple method for the functionalization of commercial glass-bottom 96-well plates through mild treatment of the materials with aqueous or ethanol solutions of poly-D-lysine (PDL) and photocleavable PEG (PCP) (Fig. 1).

PDL is a cationic polyelectrolyte that is soluble in water and can be easily adsorbed onto negatively-charged surfaces, such as glass. Its ability to enhance cell adhesion has contributed to its wide-spread use as a surface modification agent for cell culture substrate.[8,53] PCP, on the other hand, possesses a photocleavable 2-nitrobenzyl ester and a terminal succinimidyl carbonate group and can be dissolved easily in water and ethanol. In previous work, we have demonstrated that PCP can transform amino-terminated surfaces into dynamic, photoactivatable platforms.[49] In short, this is achieved by introducing PEG to amino-terminated surfaces via the reaction of the succinimidyl carbonate group, resulting in an initially non-cell-adhesive PEG surface. Upon near-UV irradiation, the photocleavage of the 2-nitrobenzyl group releases the PEG chains, triggering the surface to become cell-adhesive. The efficacy of the PEG-tethered surface for resisting cell and protein adsorption is strongly influenced by the density of the PEG chains. Successive treatment of longer and shorter PEG chains (mixed-PEG surface) have been shown to drastically enhance the surface's non-biofouling nature, due to the significant increase in PEG chain density by filling the gaps between the longer PEG chains.[54] Thus, the mixed-PEG surface based on two different PCPs showed an excellent switching efficiency in cell adhesiveness by photoirradiation.[49] The

multiplex feature of the prepared photoactivatable 96-well plate based on PDL and PCP allowed for the facile preparation of the dose-response curve of a model drug and determination of its 50%-dose inhibitory concentration (IC_{50}) value against cell migration. Furthermore, the dependency of the efficacy of another model drug on migrating environments was clearly demonstrated by studying cell migration along controlled geometrical constraints. The preparation and the functionalities are discussed in detail below.

Materials and methods

Materials

α-Methoxy-ω-azide-poly(ethylene glycol) (MeO-PEG-N$_3$; M_n=2,000 or 5,000) was purchased from Iris Biotech (Marktredwitz, Germany). Copper bromide(I) (CuBr(I)), acetonitrile (CH$_3$CN), diethyl ether, benzene, methanol (MeOH), ethanol (EtOH), dimethyl sulfoxide (DMSO), penicillin-streptomycin, cytochalasin D, and blebbistatin were purchased from Wako Pure Chemical Industries (Osaka, Japan). Metal scavenger (Quadrapure TU), poly-D-lysine (PDL; M_w= 30,000-70,000), fluorescein isothiocyanate-labelled bovine serum albumin (FITC-BSA), Minimum Essential Medium (MEM), and L-glutamine were purchased from Sigma-Aldrich (St Louis, MO, USA). Fetal bovine serum (FBS) was purchased from BioWest (Nuaille, France). MEM Non-essential amino acids and Trypsin-EDTA solution were purchased from Invitrogen (Carlsbad, CA, USA). Glass coverslips was purchased from Matsunami (0.12−0.17 mm thick, Osaka, Japan). 96-well glass bottom plates were purchased from Thermo Scientific (NY, USA). All chemicals were used without further purification.

Synthesis of Photocleavable PEG

Photocleavable PEG (PCP) was synthesized from MeO-PEG-N$_3$ and a photocleavable linker, 1-(5-methoxy-2-nitro-4-prop-2-ynyloxyphenyl)ethyl N-succinimidyl carbonate, via the Cu(I)-catalyzed Huisgen 1,3-dipolar cycloaddition (click chemistry) as described in our previous report with slight modification.[49] The synthesized PCP polymers are called PCP5k and PCP2k, depending on the molecular weight of MeO-PEG-N$_3$. PCP5k was synthesized as follows. Briefly, MeO-PEG-N$_3$ (M_n=5,000, 0.04 mmol), 1-(5-methoxy-2-nitro-4-prop-2-ynyloxyphenyl)ethyl N-succinimidyl carbonate (0.044 mmol) and CuBr(I) (0.044 mmol) were weighted into flask and dissolved in 10 mL of CH$_3$CN. The reaction was conducted for 5 h at 50°C under a nitrogen atmosphere. After the reaction, 500 mg of Quadrapure TU (beads of porous polystyrene functionalized with thiourea moieties) was added to the reaction mixture and stirred overnight to remove Cu(I) ions. Then, Quadrapure TU was removed by filtration. The resulting polymer was purified by repeating precipitation into diethyl ether for 3 times. The recovered polymer was finally freeze-dried with benzene to obtain PCP5k. PCP2k was synthesized from MeO-PEG-N$_3$ (M_n=2,000) in the same procedure, except for the concentration of each compound being 2.5 times.

Surface functionalization

Glass coverslips or glass-bottom 96-well plates were rinsed with MeOH for 3 times and dried with nitrogen. PDL (1 mg/mL) was deposited onto the glass surface from its NaCl solution (150 mM) for 3 h at 50°C. The PDL-adsorbed glass surfaces were then washed with ultra-pure water for 3 times and dried with nitrogen. The surface was soaked in an EtOH solution containing PCP5k (1 mg/mL) and reacted overnight at 50°C. Unreacted polymer was removed from the surface by washing 3 times with EtOH. Next, the surface was treated with a PCP2k solution in EtOH (1 mg/mL) in a similar fashion. The obtained PCP5k/2k-PDL-modified surfaces were kept in ultra-pure water prior to use.

Photoirradiation of the substrates

For the ζ-potential and contact angle measurements, PEGylated surfaces were irradiated with a mercury arc lamp (Optical Modulex, Ushio, Tokyo, Japan) through a UV-transmitting filter (U330, Hoya, Tokyo, Japan) and washed in PBS. For the protein adsorption and cell patterning studies, PEGylated surfaces were irradiated under an IX81-PAFM fluorescence microscope (Olympus, Tokyo, Japan) equipped with a UPLSAPO 10× objective lens (Olympus) and an excitation filter (377 ± 25 nm; Omega, Brattleboro, VT). The power density of the UV light was measured with a UIT-150 power meter equipped with a UVD-S365 (Ushio). The irradiation dose was kept at 10 J/cm^2, where the photocleavage reaction of the 2-nitrobenzyl ester is almost completed based on our previous study.[49] The photoirradiation pattern was controlled by inserting a photomask printed on a transparency at the position of the field diaphragm.[44,45,52] The functionalized glass coverslip was cut into pieces (*ca.* 100 mm^2), and one of them was placed in a 35-mm glass-bottom dish (MatTek, MA, USA) and soaked in PBS for the irradiation. On the other hand, the functionalized glass-bottom dish was directly irradiated by filling the well with PBS. Photoirradiation procedure for cell migration induction is described below.

ζ-potential measurement

The surface charge of the glass coverslip substrates was measured by ζ-potential analyzer (Delsa Nano C, Beckman Coulter, CA, USA) equipped with a flat surface cell. The monitoring polystyrene particles were suspended in 10 mM NaCl (pH7.0) and the mobility of the particles under an electric field was detected along the vertical direction toward the center of the sample cell by using the Doppler shift of the laser.

Contact angle measurement

Contact angles of water on the prepared surfaces were measured using a contact angle analyzer (DropMaster 500, Kyowa Interface Science, Niiza, Japan). The liquid droplet was gently placed onto the surface of the glass coverslip substrate and monitored with a charge-coupled device (CCD) camera. The captured images were analyzed using FAMAS software (Kyowa Interface Science) to determine the contact angle.

Quantitative analysis of protein adsorption

The protein adsorption on the surface was evaluated using FITC-BSA as a model protein. FITC-BSA (1 mg/mL in PBS) was deposited on the sample surfaces and kept for 3 h at room temperature. After washing with PBS for 5 times, fluorescence

images were captured with a cooled CCD camera (Retiga-Exi, Q-Imaging, Burnaby, BC, Canada) under a fluorescence microscope using the following set of barrier filters (Omega): 485DF15, 505DRLPXR, and 510AF23. The obtained fluorescence images were analyzed using the MetaMorph image processing system (Molecular Devices, Downingtown, PA) and the amount of adsorbed FITC-BSA was evaluated based on the fluorescence intensity after background subtraction.

Cell culture, patterning, and migration induction

Madin Darby canine kidney (MDCK) epithelial cells were cultured at 37°C, 5% CO_2 in MEM supplemented with 10% heat inactivated FBS, 1% MEM Non-Essential Amino Acids, 1% Penicillin-Streptomycin and freshly added L-glutamine. For passaging and prior to the experiments, cells were detached with a Trypsin-EDTA solution. For the cell patterning, cells were seeded onto the photoirradiated surfaces at 1×10^6 cells/dish and 2×10^4 cells/well for the glass-bottom dishes and the 96-well plate, respectively. These seeding densities correspond to 1×10^5 cells/cm^2 and 6×10^4 cells/cm^2. Unattached cells were removed after 2 h by replacing the medium. Cells were treated with cytochalasin D or blebistatin after culturing the cells for 6 h and 24 h, respectively. Then, cell migration was induced either by irradiating the entire regions of the surface for the cluster expansion experiments or by irradiating rectangular shaped regions (width = 20 or 200 μm) alongside the patterned cells[52] for studying cell migration along geometrical constraints, both for 10 J/cm^2. This irradiation dose has been demonstrated to have little cytotoxicity in our previous report.[49] Cell migration was imaged by the above-mentioned microscope at given time points and analyzed using the MetaMorph software. Cell migration profiles were examined in terms of mean cluster area or displacement of the cluster front.

Results and discussion

Surface characterization

In this study, we engineered a photoactivatable platform by successively adsorbing PDL and conjugating PCP to commercial glass-bottom 96-well plates. In order to monitor the functionalization process of this system, we analyzed the surface chemistry change of standard glass coverslips treated with the identical protocol for functionalizing 96-well plates. Because of different charges of glass surface and PDL, and their masking by the subsequent PEGylation, we believe the ζ-potential is the most useful measure for surface functionalization in our scheme. Moreover, it should be emphasized that we already know that ζ-potential is the essential factor that determines the surface photoswitchability for cell adhesion from our previous study.[51] Fig. 2A illustrates the changes in ζ-potential throughout the functionalization procedure. To start, the ζ-potential of the bare glass was about -30 mV (Fig. 2A(i)) and, upon modification by PDL, it increased to +65 mV (Fig. 2A(ii)). This result represents the negatively-charged glass surface being coated by the positively-charged PDL via electrostatic interactions. In contrast, the ζ-potential dropped close to zero upon addition of PCP5k to the
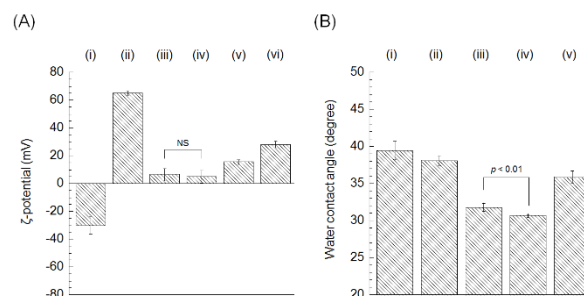
Fig. 2 Surface characterizations of photoactivatable glass coverslip substrate. (A) ζ-potential and (B) contact angle measurement results of (i) bare-glass, (ii) PDL-modified glass, (iii) PCP5k-PDL-modified glass, (iv) PCP5k/2k-PDL-modified glass, (v) PCP5k/2k-PDL-modified glass after photoirradiation for 10 J/cm^2, and (vi) PCP5k/2k-PDL-modified glass after photoirradiation for 20 J/cm^2. The data presented as mean±SD (n=3) (NS indicates not significant). Statistical significance (P<0.01) was evaluated using Student's t-test.
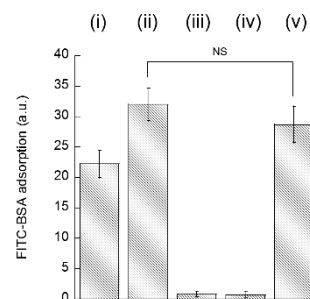
Fig. 3 FITC-BSA adsorption changes during PEGylation and photocleavage reactions on the photoactivatable glass coverslip substrate. (i) Bare-glass, (ii) PDL-modified glass, (iii) PCP5k-PDL-modified glass, (iv) PCP5k/2k-PDL-modified glass, and (v) PCP5k/2k-PDL-modified glass after near-UV irradiation. FITC-BSA concentration: 1 mg/mL. The data presented as mean±SD (n=3) (NS indicates not significant). Statistical significance (P<0.01) was evaluated using a two-tail Student's t-test.

PDL-modified glass (Fig. 2A(iii)). This suggests that the PCP5k conjugated successfully to the PDL glass surface, allowing the PEG chains to be tethered from the surface and extend into the aqueous environment to shield the surface charge. The ζ-potential of the mixed PCP5k/2k-PDL-modified surface became slightly closer to zero but stayed within statistical errors of that of the PDL-modified surface functionalized with PCP5k alone (Fig. 2(A)(iv)). The evidence for the successful conjugation of PCP2k to the empty space of the PCP5k-PDL-modified surface will be discussed in the following contact angle study (*vide infra*). Additionally, the ζ-potential values of PCP5k/2k-PDL-modified glass were almost identical for 3 h and overnight reactions (data not shown), so PEGylation is sufficiently completed by the overnight reaction.

Surface modifications to the glass surface were also evaluated using contact angle measurements. The contact angle values of the bare glass (Fig. 2B (i)) and PDL-modified glass (Fig. 2B (ii)) were similar, whereas it slightly decreased upon
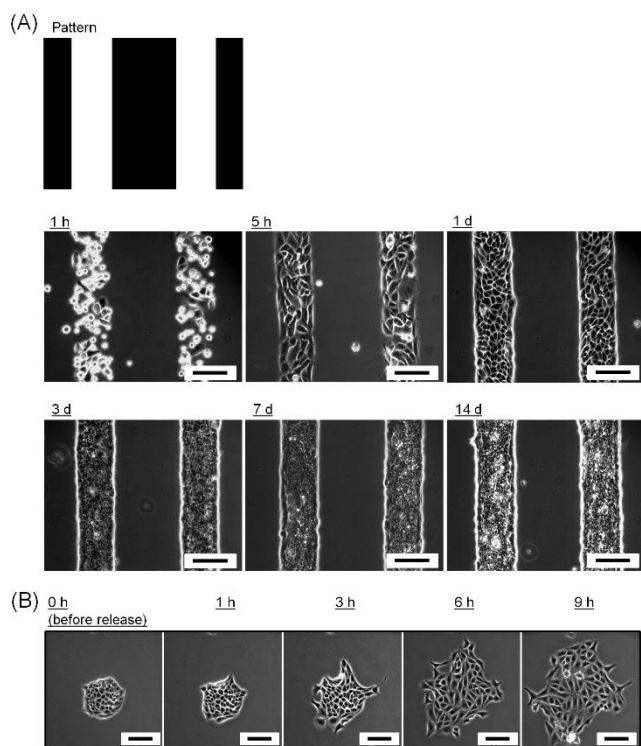
Fig. 4 Spatiotemporal control of cell adhesion on the photoactivatable glass coverslip substrate. (A) Cell patterning on the substrate. MDCK cells were allowed to attach in a striped pattern for 1 h and then cultured for 14 days. Phase-contrast images after given times are shown. (B) Cell migration induction from a geometrical confinement. MDCK cells were patterned in a circular spot and their migration was induced by the secondary irradiation of the entire surface at 24 h after cell seeding. Scale bars: 100 μm.

PEGylation with PCP5k (Fig. 2B (iii)) and PCP2k (Fig. 2B (iv)). These results are in good agreement with the previously reported contact angle values of PEG-modified surfaces.[55] Especially, the fact that contact angle value of the mixed PCP5k/2k-PDL-modified surface is statistically-significantly lower than that of the PCP5k-PDL-modified glass surface suggests that PCP2k was successfully grafted between PCP5k brushes, and hence the mixed PEG surface possesses a higher PEG density.

Next, the photoactivatable feature of the surface was evaluated by using the same two surface analysis methods. Photoirradiation against the PCP5k/2k mixed surface for 10 J/cm^2 increased the ζ-potential and contact angle value (Fig. 2A(v) and Fig.2B(v), respectively). However, the values did not completely overlap with those of the PDL-modified surface. We suppose two possibilities for this reason: (1) The photoirradiation time is insufficient for the complete cleavage of PCP from the surface. Actually, when we increased the irradiation dose to 20 J/cm^2, we observed further elevation of the ζ-potential value (28 mV, Fig.2A (vi)), which is still lower than the PDL-coated surface (65 mV, Fig.2A(ii)). We do not expect further progress of the reaction as our previous study demonstrated the photocleavage reaction completed within 10–20 J/cm^2.[49] (2) The second possibility is that some portion of weakly adsorbed PDL dissolute to the bulk solution in the PDL-g-PEG form during the PCP functionalization steps, hence the

ζ-potential value did not completely recover to the original value. Although these surface analyses indicate that the photoirradiated surface is not completely identical to the original PDL-coated surface, it should be emphasized that the photoactivatable feature is successfully introduced to the glass surface by this functionalization procedure. Moreover, the following studies support that the surface regains protein-adsorbing and cell-adhesive properties comparable to the original PDL-coated surface after photoirradiation for 10 J/cm^2. This feature is practically most important aspect for the cell migration assay platform, therefore we used 10 J/cm^2 for the following studies. Moreover, it should be emphasized complete restoration of the original PDL-coated surface after PEG photorelease is not required for the purpose discussed in this paper. It becomes more obvious when our method is compared with conventional scratch wound healing assay.[17-20] In this widely used golden standard, one portion of confluent cell monolayers was scratched to induce cell migration. The scratching process produces cell debris of dead cells, and hence the cells have to migrate over the uncontrollable stuff. Compared to this conventional method, our approach yields chemically much cleaner surfaces after photoirradiation and the migration experiments were carried out on the surfaces with identical conditions.

Because cell adhesion is largely mediated by surface-adsorbed proteins, we investigated the change in protein-repelling ability of the substrates during the functionalization procedure by using FITC-BSA as a model protein. Fig. 3 illustrates the FITC-BSA adsorption amount of (i) bare glass, (ii) PDL-modified glass, (iii) PCP5k-PDL-modified glass, (iv) mixed PCP5k/2k-PDL-modified glass, and (v) the same mixed PCP5k/2k-PDL-modified glass irradiated with near-UV light. PDL-modified glass showed higher protein adsorption as compared with bare glass due to the attraction of the negatively-charged protein to the positively-charged surface (Fig. 3 (i) and (ii)). On the other hand, protein adsorption was drastically decreased by PEG modification (Fig. 3 (iii) and (iv)), suggesting that the PEG chains prevented protein adsorption on the surface by steric repulsion. Additionally, photoirradiation against the PCP5k/2k mixed surface returned the protein adsorption level close to those before PEG modification (Fig. 3 (v)). From this data, we concluded that the photo-responsive feature was successfully introduced on the glass surface by using PCP. In agreement with the ζ-potential results above, the amount of adsorbed protein was much lower for the PDL-modified glass functionalized with PCP5k and PCP2k than that for PCP5k alone. These results emphasize the significance of backfilling with PEG2k for complete blocking of protein adsorption as discussed in our earlier report.[51] Thus, for the remaining studies, we focused on substrates functionalized with mixed PCP, PCP5k and PCP2k, and hereafter we will refer to this substrate as "PEGylated" surface.

Next, we examined the change of cell adhesion on the PEGylated glass surface before and after near-UV irradiation. The PEGylated surface was irradiated in a striped pattern in PBS by projection exposure under a fluorescence microscope (Fig. 4A).[44,45,52] After washing the substrate with PBS, MDCK cells were allowed to attach to the surface. Cells were selectively adhered to the irradiated regions within 2 h and confined within the regions for at least 2 weeks (Fig. 4A). Therefore, the obtained cellular pattern on the substrate demonstrated high stability and potential for long-time studies. Furthermore, a proof-of-concept experiment for the application of the PEGylated substrate for cell migration studies was

demonstrated in Fig. 4B. In this particular case, the PEGylated substrate was irradiated in a circle pattern by projection exposure under a fluorescence microscope. Cells adhered selectively to the irradiated circle region, and the cells became confluent within the initial circular cluster at 24 h after seeding (Fig. 4B, 0 h (before release)). Then, migration was induced by irradiating the entire surface. The cellular cluster expanded in a radial fashion toward the previously idle areas. It should be noted that this dose of near-UV irradiation has little cytotoxicity, which has been demonstrated in our previous paper.[49] Overall, the surface functionalization protocol described above allows for the transformation of glass substrate into photoactivatable surface. With this technology, we demonstrated the ability to pattern cells in defined geometries and induce their migration by activating regions adjacent to the patterned cells by secondary photoirradiation.

Multiplex cell migration assay on photoactivatable 96-well plates

Next, we functionalized the surface of glass-bottom 96-well plates in an identical fashion to that of glass coverslips and evaluated the capability for multiplex cell migration assay and drug testing. For a proof-of-concept, we selected a circular pattern of 400 μm diameter for the initial cell cluster geometry, since it is easy to quantitatively evaluate cell migration from the increase in the cluster area. For our model drug, we selected cytochalasin D, an inhibitor of actin polymerization, and thus cell migration.

Analogous to the glass coverslips, we obtained similar circular cellular patterns within the wells of the 96-well plates (Fig. 5A, 0 h, 0 μM). Precise circular patterns were formed in about 70% of the wells, and the number of cells within the initial clusters was 170 ± 20 cells/cluster. A few round cells seen in the surrounding regions are non-specifically attached cells, which were difficult to remove by medium change in this experiment. However, the number of non-specifically attached cells that stayed within the regions of the cluster expansion is sufficiently lower (*ca.* 5%) than the variation of the number of cells of the initial clusters. Therefore, their contribution to the cell area increase is almost negligible. On the other hand, in the remaining 30% of the wells, the cell clusters were larger than initial irradiated area. This is because, in the case of the 96-well plates, excess cells remain in the solutions, eventually resulting in non-specific adhesion to the non-irradiated area. We did not use these wells for the further experiments. However, the yield of the circular pattern formation is expected to be improved by optimizing cell seeding density and the timing of the medium change after cell seeding, or by photopatterning additional cell-adhesive regions at the periphery of each well, where excess cells can adhere.

Fig. 5A demonstrates examples of cell migration behavior of cells before (left) and 12 hours after (right) release of geometrical confinement under different cytochalasin D concentrations (0–10 μM). Simultaneous drug screening (18 wells) with different drug concentration was carried out. We observed a gradual decrease in the cluster expansion when increasing the cytochalasin D concentration. Especially, under high cytochalasin D concentrations (1 μM and 10 μM), cells hardly migrated. These results indicate that cell migration was effectively inhibited by cytochalasin D within this concentration range. From the dose response curve plotted in Fig. 5B, the 50% inhibitory concentration (IC_{50}) value of cytochalasin D was calculated to be 0.015 μM. Joy *et al.*
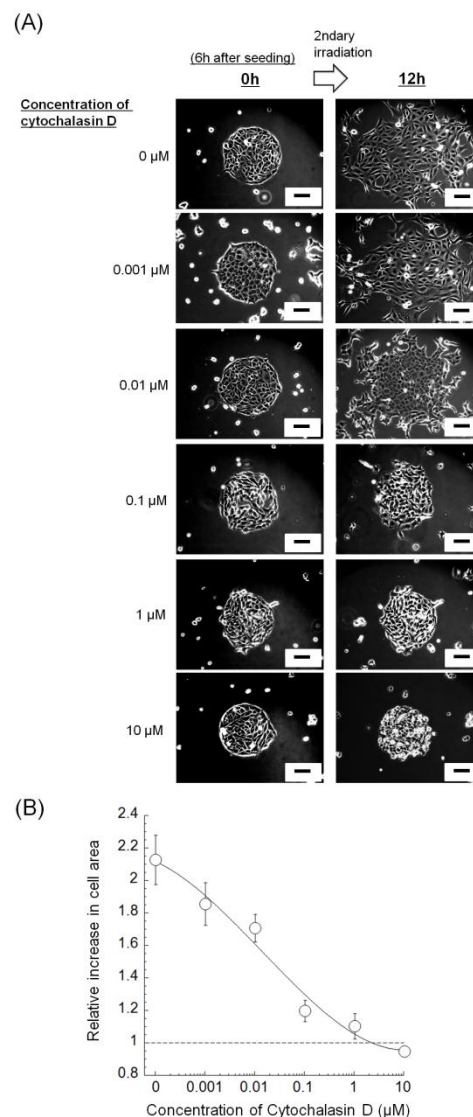
Fig. 5 Multiplexed cell migration assay on the photoactivatable glass-bottom 96-well plate for the evaluation of IC_{50} of a model drug. (A) Cytochalasin D concentration dependent cell migration behaviors of the cells before (left, 0 h) and after (right, 12 h) release of geometrical confinement. MDCK cells were confined within circular spots and their migration was induced by the secondary irradiation at 6 h after cell seeding. Scale bars: 100 μm. (B) Dose-response curve constructed from three independent experiments for the cell migration behavior of MDCK cells exposed to cytochalasin D. Relative increase in mean cell area during 12 h migration is plotted against each cytochalasin concentration. The data presented as mean±SD (n=3).

reported that the IC_{50} value of cytochalasin D for the migration of human breast cancer cells was 0.078 μM.[56] Our results showed the same order value, and therefore it is within acceptable agreement with this report, considering the different cell lines used in these studies. Moreover, the Z'-factor of our cell migration assay was calculated from cytochalasin D screening experiments. Z'-factor serves as an indicator for the reliability of HTS techniques.[57] Generally, HTS techniques

with a Z'-factor between 0.5 and 1.0 are considered highly-reliable. The Z'-factor is defined as follows:

$$Z' = 1.0 - (3.0 \times (SD_{nc} + SD_{pc})/|AVE_{nc} - AVE_{pc}|)$$

SD_{nc} and SD_{pc} are the sample standard deviation (SD) of the

negative (0 μM cytochalasin D) and positive controls (10 μM cytochalasin D), respectively, and AVE_{nc} and AVE_{pc} are the average value of positive and negative controls, respectively. From the results of cytochalasin D screening, the Z'-factor value for our system was calculated to be 0.53 (n = 3), and this value is within the range for reliable HTS techniques. Taken
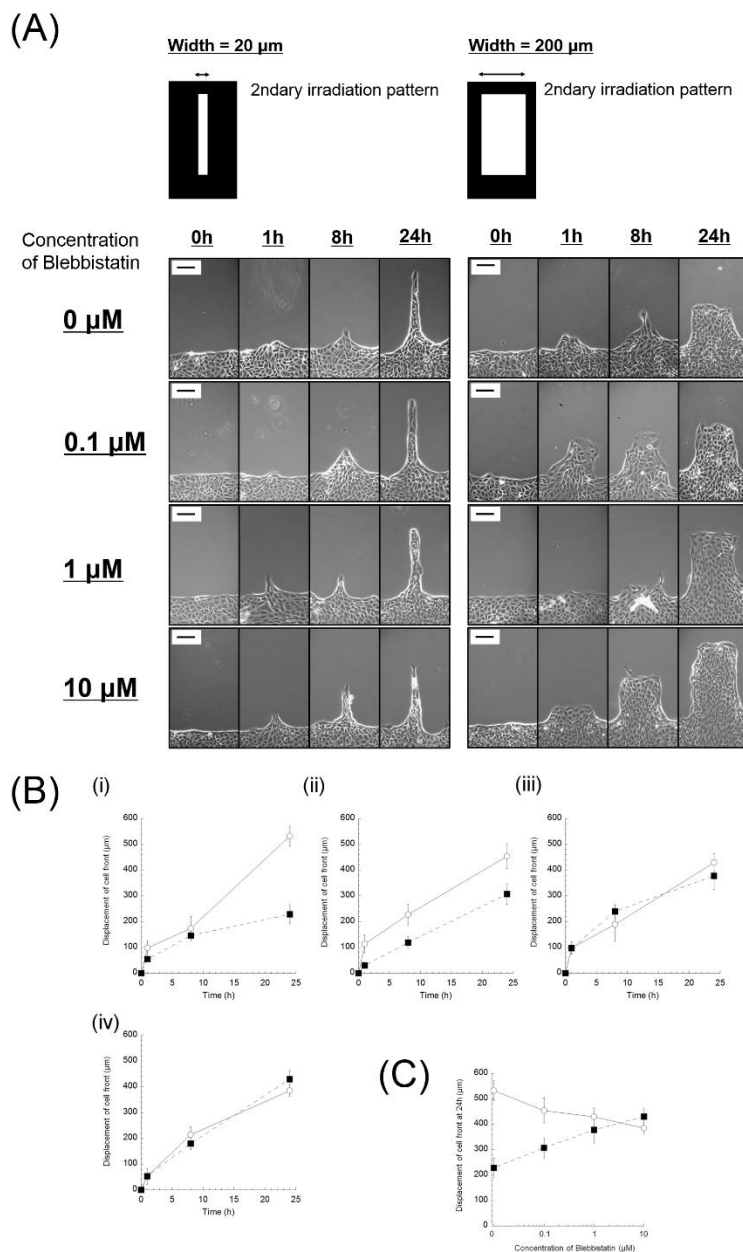
Fig. 6 Multiplexed cell migration assay in controlled geometrical constraints on photoactivatable glass-bottom 96-well plate. (A) Blebbistatin concentration dependent cell migration behavior of MDCK cells before and after inducing cell migration along given geometrical constraints. MDCK cells were patterned in large cell-adhesive regions and their migration was induced by the secondary irradiation at 6 h after cell seeding. Scale bar: 100 μm. (B) Time dependent cell migration profiles at different blebbistatin concentrations. Blebbistatin concentration : (i) 0 μM, (ii) 0.1 μM, (iii) 1 μM, and (iv) 10 μM, respectively. Width of secondary irradiation pattern: 20 μm (Open circles) and 200 μm (filled square). (C) Blebbistatin concentration dependent displacement of cell front at 24 h after secondary irradiation. Width of secondary irradiation pattern: 20 μm (Open circles) and 200 μm (filled square). The data presented as mean±SD (n=3).

together, we are able to conclude that our method enables accurate and precise screening of drugs that regulate cell migration.

Finally, we examined the impact of cell migrating environments on the potency and efficacy of another model drug. Ladoux and colleagues reported on the existence of distinct collective migration modes, contraction-elongation type motion and smooth migration with large-scale vortices over tens of cell lengths, which depend on the geometrical constraints. This dependency diminished through a loss of cell contractility when treated with the myosin II inhibitor, blebbistatin.[14] On the basis of this report, we hypothesized that such cell-cell interaction modifiers may act on cells differently depending on their migrating environments.

The PEGylated glass bottom plate was irradiated to create large cell-adhesive regions by projection exposure under a fluorescence microscope, whereby MDCK cells were selectively allowed to attach (Fig. 6A, 0 h). After adding blebbistatin (0–10 μM) to each well, rectangular regions with different widths (20 and 200 μm) were irradiated adjacent to the initial cell cluster to induce their migration within the geometrical constraints. Fig. 6A shows the cell migration behavior of cells before and after inducing cell migration under different blebbistatin concentrations. Simultaneous drug screening (24 wells) with different drug concentration and widths of migration paths was carried out. For all of the examined blebbistatin concentrations and the widths of migration paths, cells showed time-dependent migration. The displacement of the cell fronts were plotted in Fig. 6B(i)–(iv). Without blebbstatin treatment, the cells traveled longer distances along the narrow path (20 μm, Fig. 6B(i) open circles) than the wide path (200 μm, Fig. 6B(i) filled squares) after 24 hours of incubation. The difference between the travelled distances between the two paths became smaller as blebbistatin concentrations increased and became almost negligible at the highest concentrations (Fig. 6 B(iv)). The distinct impact of blebbistatin on cells migrating along different path widths becomes more apparent when comparing their dose-response curves (Fig. 6C). These graphs show that blebbistatin retards cells migrating along the narrow path (20 μm), whereas it accelerates those along the wide path (200 μm). Ladoux and coworkers demonstrated that the treatment of blebbistatin resulted in the loss of vortex formation as well as caterpillar-like motions in cell monolayers by inhibiting acto-myosin contractility.[14] Therefore, the opposite actions of blebbistatin on cell migrating on different paths observed in our study can be caused by the possibility that while blebbistatin treatment slightly attenuates cell migration activity itself (as observed on the narrow path), the loss of vortex-formation makes cells concentrate exclusively on the forward movement, overwhelming slight delay in the migration activity and eventually resulting in faster migration on the wide path. Whatever the reason may be, the different responses to blebbistatin (depending on migration geometries) strongly highlights the importance of evaluating drug efficacies and potencies in controlled geometrical constraints. It should be noted that our photoswitching approach enables studies of cell migration within precisely controlled geometries down to single cell resolutions,[47] which is difficult to achieve using exclusion zone assays.[14] Moreover, the 96-well format is convenient for constructing dose-response curves for multiple drugs within a single experiment. Therefore, the present material is anticipated as an ideal platform for high-throughput screening of drug candidates that regulate migration of single cells as well as cell

clusters in controlled geometrical constraints. Further experiments including the effect of physical ground for collective cell migration and drug efficacy are now under investigation. The detailed investigation will be published in a forthcoming paper.

Conclusions

In this paper, we designed and prepared a novel biosurface based on photocleavable PEG and PDL for cell migration-based drug screening. The surface functionalization procedure and its photoswitching capabilities were characterized by ζ-potential measurements, contact angle measurements, and protein adsorption tests by using a glass coverslip as a model substrate. The PEG-tethered substrates showed cell-resistivity and became cell-adhesive upon releasing PEG by near-UV irradiation. Cells were selectively adhered to the irradiated regions and confined within the regions for at least 2 weeks. Cell migration from the initial cell patterns was successfully induced by a second near-UV irradiation. Because of these features, cell migration from and along precisely controlled geometrical confinements became possible. Cell migration-based drug screenings were carried out using PEGylated 96-well glass bottoms with different geometrical confinements of initial cell clusters. The impact of cytochalasin D on cell migration was evaluated by observing its ability to inhibit cluster expansions, and its dose-response curve was successfully constructed. Furthermore, blebbistatin-treated cells exhibited opposite responses, either decelerating or accelerating, depending on the widths of migrating strips. These results strongly support the significance of evaluating drug efficacies under controlled migrating microenvironments. Therefore, the obtained photoactivatable 96-well plate is a promising candidate for a high-throughput cell migration assay platform.

Acknowledgements

Notes and references

[a] World Premier International (WPI) Research Center Initiative, International Center for Materials Nanoarchitectonics (MANA), National Institute for Materials Science (NIMS), 1-1 Namiki, Tsukuba 305-0044, Japan.

[b] The UC Berkeley – UCSF Graduate Program in Bioengineering, University of California, Berkeley, California, 94720, USA.

[c] Department of Chemistry, Faculty of Science, Research Institute for Photofunctionalized Materials, Kanagawa University, 2946 Tsuchiya, Hiratsuka, Kanagawa 259-1293, Japan.

1   P. Rørth, *Annu. Rev. Cell Dev. Biol.*, 2009, **25**, 407.

2   P. Friedl and D. Gilmour, *Nat. Rev. Mol. Cell Biol.*, 2009, **10**, 445.

3   J. J. Gooding, S. G. Parker, Y. Lu and K. Gaus, *Langmuir*, 2014, 30, 3290.

4   P. Friedl and K. Wolf, *Nat. Rev. Cancer*, 2003, **3**, 362.

5   E. Sahai, *Curr. Opin. Genet. Dev.*, 2005, **15**, 87.

6   P. Zengel, D. Ramp, B. Mack, S. Zahler, A. Berghaus, B. Muehlenweg, O. Gires and S. Schmitz, *BMC Cancer*, 2010, **10**, 92.

7   D. M. Timm, J. Chen, D. Sing, J. A. Gage, W. L. Haisler, S. K. Neeley, R. M. Raphael, M. Dehghani, K. P. Rosenblatt, T. C. Killian, H. Tseng and G. R. Souza, *Sci. Rep.*, 2013, DOI:10.1038/srep03000.

8   J. Silva, F Lautenschläger, C. R. Kuo, J. Guck and E. Sivani, *Integr. Biol.*, 2011, **3**, 1202.

9   I. Kola and J. Landis, *Nat. Rev Drug Discov.*, 2004, **3**, 711.

10 P. Szymański, M. Markowicz and E. Mikiciuk-Olasik, *Int. J. Mol. Sci.*, 2012, **13**, 427.

11 K. I. Hulkower and R. L. Herber, *Pharmaceutics*, 2011, **3**, 107.

12 N. Kramer, A. Walzl, C. Unger, M. Rosner, G. Krupitza, M. Hengstschläger and H. Dolznig, *Mutat Res.*, 2013, **752**, 10.

13 K. J. Simpson, L. M. Selfors, J. Bui, A. Reynolds, D. Leake, A. Khvorova and J. S. Brugge, *Nat. Cell Biol.*, 2008, **10**, 1027.

14 S. R. K Vedula, M. C. Leong, T. L. Lai, P. Hersen, A. J. Kabla, C. T. Lim and B. Ladoux, *Proc. Natl. Acad. Sci. U.S.A.*, 2012, **109**, 12974.

15 C. G. Rolli, H. Nakayama, K. Yamaguchi, J. P. Spatz, R. Kemkemer and J. Nakanishi, *Biomaterials*, 2012, **33**, 2409.

16 K, Wolf, M. te Lindert, M. Krause, S. Alexander, J. te Riet, A. L. Willis, R. M. Hoffman, C. G. Figdor, S. J. Weiss and P. Friedl, *J. Cell Biol.*, 2013, **201**, 1069.

17 Y. Kam, C. Guess, L. Estrada, B. Weidow and V. Quaranta, *BMC Cancer*, 2008, **8**, 198

18 J. C. Yarrow, Y. Feng, Z. E. Perlman, T. Kirchhausen and T. J. Mitchison, *Comb. Chem. High Throughput Screen.*, 2003, **6**, 279.

19 N. O. Carragher, *Clin. Exp. Metastasis*, 2009, **26**, 381.

20 J. C. Yarrow, Z. E. Perlman, H. J. Westwood and T. J. Mitchison, *BMC Biotechnol.*, 2004, **4**, 21.

21 A. Folch, B. H. Jo, O. Hurtado, D. J. Beebe and M. Toner, *J. Biomed. Mater. Res.*, 2000, **52**, 346.

22 E. Ostuni, R. Kane, C. Chen, D. Ingber and G. M. Whitesides, *Langmuir*, 2000, **16**, 7811.

23 M. Poujade, E. Grasland-Mongrain, A. Hertzog, J. Jouanneau, P. Chavrier, B. Ladoux, A. Buguin and P. Silberzan, *Proc. Nat. Acad. Sci. USA*, 2007, **104**, 15988.

24 M. Obara, T. Sakuma, K. Fujikawa, *J. Biochem.*, 2010, **147**, 327.

25 V. Echeverria, I. Meyvantsson, A. Skoien, T. Worzella, C. Lamers and S. Hayes, *J. Biomol. Screen*, 2010, 15, 1144.

26 I. Meyvantsson and D. J. Beebe, *Ann. Rev. Anal. Chem.*, 2008, **1**, 423.

27 S. Raghavan, R. Desai, Y. Kwon, M. Mrksich and C. Chen, *Langmuir*, 2010, **26**, 17733.

28 A W. Luo and M. Yousaf, *J. Am. Chem. Soc.*, 2011, **133**, 10780.

29 J. Kim and R. C. Hayward, *Trends Biotechnol.*, 2012, **30**, 426.

30 J. Nakanishi, *Chem. An Asian J.*, 2014, **9**, 406.

31 Y. Haraguchi, T. Shimizu, T. Sasagawa, H. Sekine, K. Sakaguchi, T. Kikuchi, W. Sekine, S. Sekiya, M. Yamato, M. Umezu and T. Okano, *Nat. Protoc.*, 2012, **7**, 850.

32 K. Nagase, A. Kimura, T. Shimizu, K. Matsuura, M. Yamato, N. Takeda and T. Okano, *J. Mater. Chem.*, 2012, **22**, 19514.

33 M. N. Yousaf, B. T. Houseman and M. Mrksich, *Proc. Natl. Acad. Sci. U.S.A.*, 2001, **98**, 5992.

34 S. Raghavan, R. A. Desai, Y. Kwon, M. Mrksich and C. S. Chen, *Langmuir*, 2010, **26**, 17733.

35 S. Sekine, H. Kaji and M. Nishizawa, *Electrochem. Commun.*, 2009, **11**, 1781.

36 D. Liu, Y. Xie, H. Shao, X. Jiang, *Angew. Chem., Int. Ed.*, 2009, **48**, 4406.

37 K. Jang, K. Sato, K. Mawatari, T. Konno, K. Ishihara and T. Kitamori, *Biomaterials*, 2009, **30**, 1413.

38 W. Luo and M. N. Yousaf, *J. Am. Chem. Soc.*, 2011, **133**, 10780.

39 S. Yamaguchi, S. Yamahira, K. Kikuchi, K. Sumaru, T. Kanamori and T. Nagamune, *Angew. Chem., Int. Ed.*, 2012, **51**, 128.

40 M. J. Hynes and J. A. Maurer, *Mol. BioSyst.*, 2013, **9**, 559.

41 A. Azioune, M. Storch, M. Bornens, M. Théryb and M. Piel, *Lab Chip*, 2009, **9**, 1640.

42 J. Nakanishi, T. Takarada, K. Yamaguchi and M. Maeda, *Anal. Sci.*, 2008, **24**, 67.

43 H. Nakayama, J. Nakanishi, T. Shimizu, Y. Yoshino, H. Iwai, S. Kaneko, Y. Horiike and K. Yamaguchi, *Colloids Surf., B.*, 2010, **76**, 88.

44 J. Nakanishi, Y. Kikuchi, T. Takarada, H. Nakayama, K. Yamaguchi and M. Maeda, *J. Am. Chem. Soc.*, 2004, **126**, 16314.

45 J. Nakanishi, Y. Kikuchi, T. Takarada, H. Nakayama, K. Yamaguchi and M. Maeda, *Anal. Chim. Acta*, 2006, **578**, 100.

46 Y. Kikuchi, J. Nakanishi, T. Shimizu, H. Nakayama, S. Inoue, K. Yamaguchi, H. Iwai, Y. Yoshida, Y. Horiike, T. Takarada and M. Maeda, *Langmuir*, 2008, **24**, 13084.

47 J. Nakanishi, Y. Kikuchi, S. Inoue, K. Yamaguchi, T. Takarada and M. Maeda, *J. Am. Chem. Soc.*, 2007, **129**, 6694.

48 Y. Kikuchi, J. Nakanishi, H. Nakayama, T. Shimizu, Y. Yoshino, K. Yamaguchi, Y. Yoshida and Y. Horiike, *Chem. Lett.*, 2008, **37**, 1062.

49 S. Kaneko, H. Nakayama, Y. Yoshino, D. Fushimi, K. Yamaguchi, Y. Horiike and J. Nakanishi, *Phys. Chem. Chem. Phys.*, 2011, **13**, 4051.

50 Y. Shimizu, H. Boehm, K. Yamaguchi, J. P. Spatz and J. Nakanishi, *PLos One*, 2014, **9**, e91875.

51 S. Kaneko, K. Yamaguchi and J. Nakanishi, *Langmuir*, 2013, **29**, 7300.

52 J. Nakanishi, *Methods in Cell Biology Part B*, 2014, **120**, 117.

53 Y. Gu, Y. Ji, Y. Zhao, Y. Liu, F. Ding, X. Gu and Y. Yang, *Biomaterials*, 2012, **33**, 6672.

54 Y. Nagasaki, *Polymer J*, 2011, **43**, 949.

55 T. Satomi, Y. Nagasaki, H. Kobayashi, H. Otsuka and K. Kataoka, *Langmuir*, 2007, 23, 6698.

56 M. E. Joy, L. L. Vollmer, K. Hulkower, A. M. Stern, C. M. Peterson, R. C. D. Boltz, P. Roy and A. Vogt, *PLoS One*, 2014, **9**, e88350.

57 J. Zhang, T. D. Y. Chung and K. R. Oldenburg, *J. Biomol. Screen.*, 1999, **4**, 67.